Structures of human dihydroorotate dehydrogenase in complex with antiproliferative agents

Shenping Liu[1], Edie A Neidhardt[2†], Trudy H Grossman[2‡], Tim Ocain[2§] and Jon Clardy[1*]

Background: Dihydroorotate dehydrogenase (DHODH) catalyzes the fourth committed step in the *de novo* biosynthesis of pyrimidines. As rapidly proliferating human T cells have an exceptional requirement for *de novo* pyrimidine biosynthesis, small molecule DHODH inhibitors constitute an attractive therapeutic approach to autoimmune diseases, immunosuppression, and cancer. Neither the structure of human DHODH nor any member of its family was known.

Results: The high-resolution crystal structures of human DHODH in complex with two different inhibitors have been solved. The initial set of phases was obtained using multiwavelength anomalous diffraction phasing with selenomethionine-containing DHODH. The structures have been refined to crystallographic R factors of 16.8% and 16.2% at resolutions of 1.6 Å and 1.8 Å for inhibitors related to brequinar and leflunomide, respectively.

Conclusions: Human DHODH has two domains: an α/β-barrel domain containing the active site and an α-helical domain that forms the opening of a tunnel leading to the active site. Both inhibitors share a common binding site in this tunnel, and differences in the binding region govern drug sensitivity or resistance. The active site of human DHODH is generally similar to that of the previously reported bacterial active site. The greatest differences are that the catalytic base removing the proton from dihydroorotate is a serine rather than a cysteine, and that packing of the flavin mononucleotide in its binding site is tighter.

Addresses: [1]Department of Chemistry and Chemical Biology, Cornell University, Ithaca, NY 14853-1301, USA and [2]Procept, Inc., 840 Memorial Drive, Cambridge, MA 02139, USA.

Present addresses: [†]Genetics Institute, Andover, MA 01810, USA, [‡]Ariad Pharmaceuticals, Cambridge, MA 02139, USA and [§]Millennium Pharmaceuticals, Cambridge, MA 02139, USA.

*Corresponding author.
E-mail: jcc12@cornell.edu

Key words: antiproliferative agents, brequinar, crystallography, dihydroorotate dehydrogenase, leflunomide, pyrimidine biosynthesis

Received: **23 August 1999**
Revisions requested: **25 September 1999**
Revisions received: **4 October 1999**
Accepted: **27 October 1999**

Published: **20 December 1999**

Structure 2000, **8**:25–33

0969-2126/00/$ – see front matter

Introduction

Although most cells meet their requirements for nucleotides by recycling existing ones, activated T cells and other rapidly proliferating cells depend heavily on *de novo* nucleotide synthesis [1–3]. In addition to DNA and RNA synthesis, rapidly proliferating human T cells require *de novo* pyrimidine biosynthesis for protein glycosylation, membrane-lipid biosynthesis, and strand-break repair [1–3]. The therapeutic potential of inhibiting *de novo* pyrimidine biosynthesis at the dihydroorotate dehydrogenase (DHODH) catalyzed step was revealed by the antiproliferative agents leflunomide and brequinar [4,5] (Figure 1). Both compounds and many analogs are potent and selective inhibitors of mammalian DHODH [4,5]. The inhibitory mechanisms of leflunomide, which was recently approved for the treatment of rheumatoid arthritis, and brequinar, which was in clinical trials for cancer and host-versus-graft disease, are not known [6–10]. To define the structural basis of the potency and specificity of inhibitors related to both leflunomide and brequinar we have determined the high-resolution (1.6–1.8 Å) crystal structures of human DHODH in complex with A771726, the active form of leflunomide, and a brequinar analog. These structures reveal the common binding region shared by each inhibitor.

DHODHs, which catalyze the only redox step in pyrimidine biosynthesis, are divided into two large families, and the mammalian enzymes form a tightly clustered group in family *2* [11] (Figure *2*). Oxidation of dihydroorotate (DHO) to orotate (ORO) and reduction of flavin mononucleotide (FMN) to dihydroflavin mononucleotide ($FMNH_2$) comprise the two half reactions of the redox couple (Figure 1a). In family 1 DHODHs, oxygen or some water-soluble molecules such as fumarate or NAD^+ oxidize $FMNH_2$ to regenerate FMN, and the enzymes are cytosolic [12]. For human DHODH, ubiquinone is the oxidant (Figure 1a), and the enzyme associates with the mitochondrial inner membrane [1]. Full-length human DHODH has 396 residues [13] and the construct used in this work, which lacks the mitochondrial signal peptide, comprises Met30 to the C terminus (Figure *2*). This construct has full enzymatic activity, remains membrane associated, and retains brequinar sensitivity [14].

High-resolution crystal structures of human DHODH in complex with a brequinar analog and the active metabolite of leflunomide (A771726) have been solved. Although the overall α/β-barrel structure resembles a bacterial family 1 DHODH structure, there are significant differences in the

Figure 1

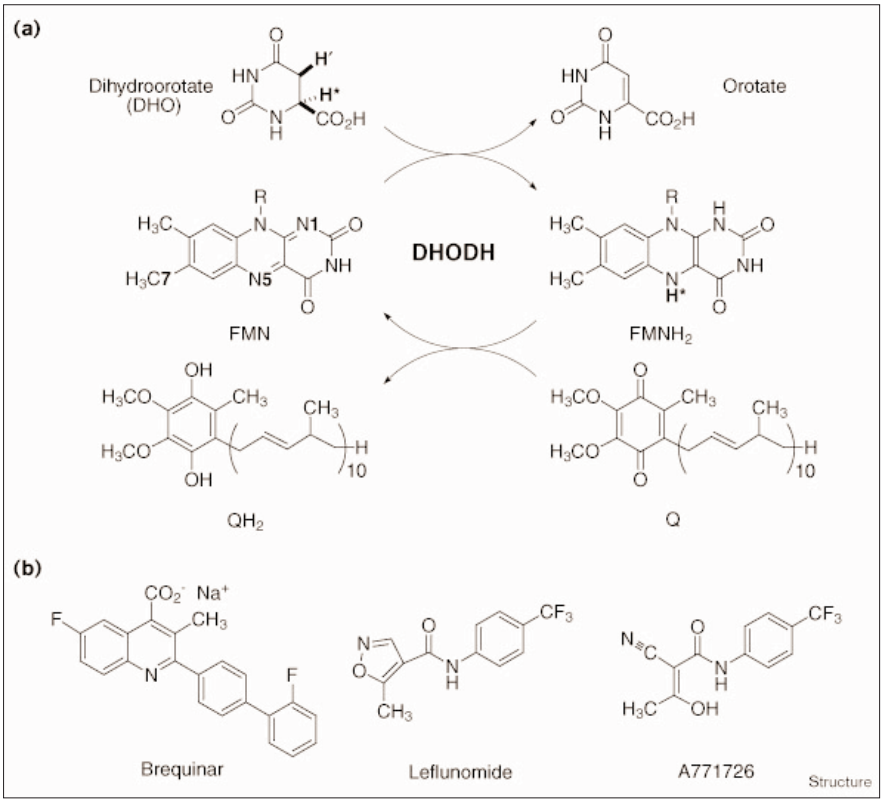

Reactions and inhibitors of human dihydroorotate dehydrogenase. **(a)** The reactions occurring in the proximal and distal redox sites of human dihydroorotate dehydrogenase (DHODH). The hydrogen denoted as H* is transferred to FMN as a hydride, and the hydrogen denoted H′ is lost as a proton. **(b)** Chemical structure of the inhibitors brequinar, leflunomide, and A771726, which is the active metabolite of leflunomide.

active site and the N-terminal extension [15,16]. In human DHODH serine replaces the cysteine catalytic base of the bacterial DHODH. The basicity of the serine seems to be enhanced by a hydrogen bond to a water that is bound to the face of an aromatic ring. The long N-terminal extension, which characterizes the membrane-bound DHODHs, folds into a helical domain that forms the entrance of a tunnel leading into the active site. The helical domain seems to be responsible for the membrane association of human DHODH. Both the brequinar analog and A771726, the leflunomide active metabolite, bind in the same region of this tunnel: a constriction near the flavin mononucleotide.

Results and discussion

The overall structure

The enzyme contains two domains connected by an extended loop: a small N-terminal domain (Met30–Leu68) and a large C-terminal domain (Met78 to the C terminus) (Figure 3). The large domain has an α/β-barrel fold with a central barrel of eight parallel β strands (β1–β8) surrounded by eight α helices (α3, α4, α6–α10 and α12) (Figure 3). At the top of the barrel three short antiparallel β strands βC, βD and βE) form a rigid side for the proximal redox site (Figure 3). A pair of antiparallel β strands, βA and βB, are at the bottom of the barrel (Figure 3). The small N-terminal domain consists of two α helices, α1 and α2, and a short loop connecting them. It packs against the α/β barrel at the side close to βC and βD (Figure 3). The extended loop, which has few interactions with the rest of the protein, connects the C terminus of α2

Figure 2

Multiple sequence alignment of selected DHODH sequences. Residues are colored based on the degree of sequence conservation: red, identical in all DHODH sequences; blue, identical residue in family 2; cyan, similar residues in all DHODH sequences; and green, identical residues in family 1. Secondary structures are also labeled. The red triangle indicates the catalytic base. Residue numbering is based on human DHODH. The alignment was made with CLUSTALW [32] and manually corrected. The figure was prepared using the program ALSCRIPT [33]. The sequences used in the alignment are HUMAN (human), RAT (rat), DROME (*Drosophila melanogaster*), RATH (*Arabidopsis thaliana*), (SCHPO) (*Schizosaccharomyces pombe*), AGRAE (*Agrocybe aegerita*), ECOLI (*Escherichia coli*), SALTY (*Salmonella typhimurium*), HAEIN (*Haemophilus influenzae*), SYNY3 (*Synechocystis* sp.), MYCLE (*Mycobacterium leprae*), LACLA (DHODH A from *Lactococcus lactis*), YEAST (yeast), LACLB (DHODH B from *Lactococcus lactis*), ENTFA (*Enterococcus faecalis*), BACCL (*Bacillus caldolyticus*), BACSU (*Bacillus subtilis*), LACPL (*Lactobacillus plantarum*), AQUAE (*Aquifex aeolicus*), METJA (*Methanococcus jannaschii*), METTH (*Methanobacterium thermoautotrophicum*), ARCFU (*Archaeoglobus fulgidus*), and SULSO (*Sulfolobus solfataricus*).

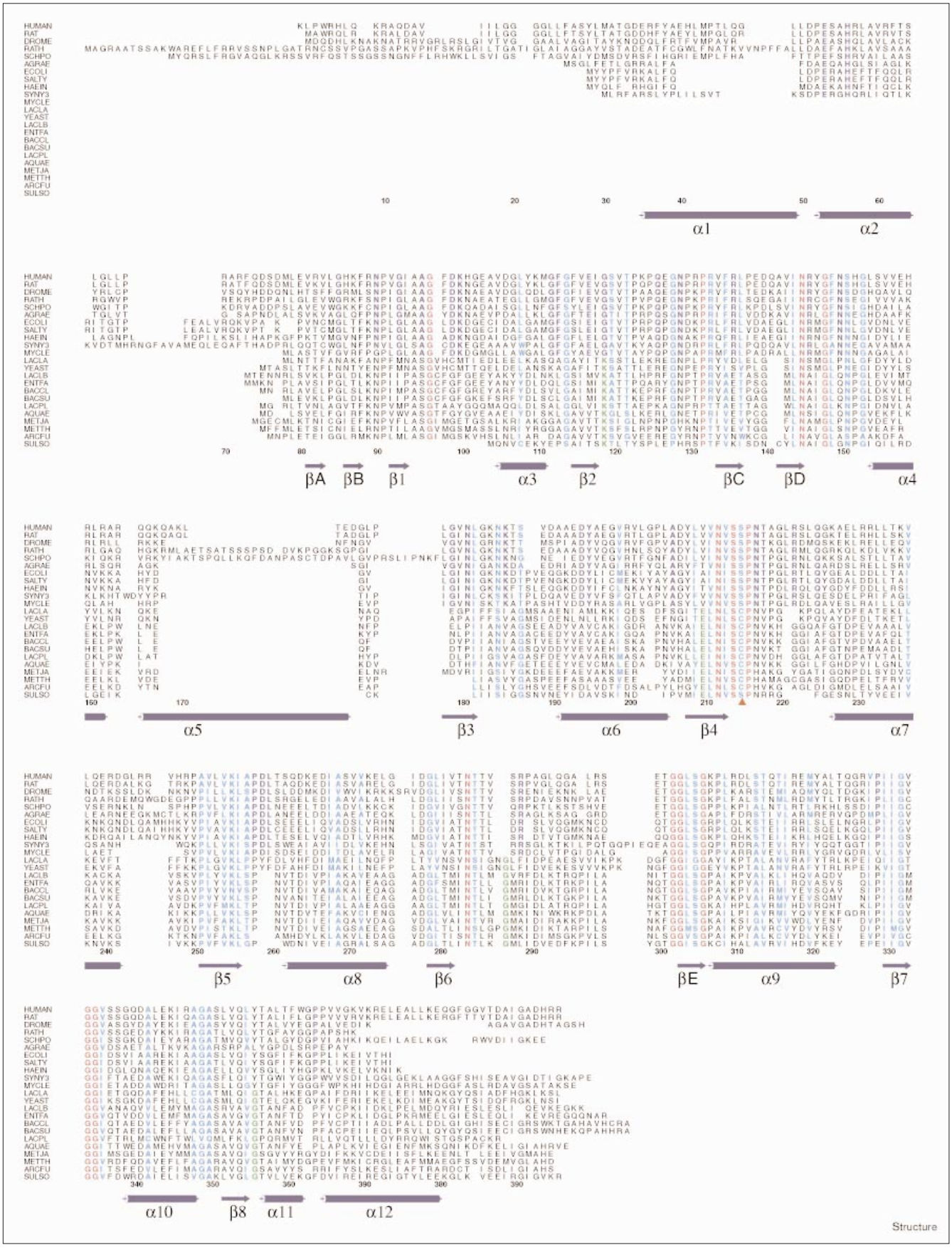
HUMAN
RAT
DROME
RATH
SCHPO
AGRAE
ECOLI
SALTY
HAEIN
SYNY3
MYCLE
LACLA
YEAST
LACLB
ENTFA
BACCL
BACSU
LACPL
AQUAE
METJA
METTH
ARCFU
SULSO
α1
α2
βA
βB
β1
α3
β2
βC
βD
α4
α5
β3
α6
β4
α7
β5
α8
β6
βE
α9
β7
α10
β8
α11
α12
Structure

to the bottom of the α/β barrel (Figure 3). The large domain has three *cis*-peptide bonds, and two of them, the *cis* bonds starting at Gly119 and Val282, seem to be necessary for FMN binding.

The overall fold of the large domain is very similar to that of *Lactococcus lactis* DHODH [15], a family 1 protein with 16% sequence identity to human DHODH (Figure 2). The *Lactococcus* enzyme exists as a dimer both in solution and in the crystal, whereas the human enzyme is a monomer in solution (based on analytical gel filtration chromatography data, not shown) and in the crystal. The root mean square deviation (rmsd) for 256 C_α positions between the two structures is 1.8 Å, and the two *cis* peptide bonds essential for FMN binding are found in both structures. The largest rms differences between the two structures are informative. The region Phe98–Val105 (β1–α3 loop) interacts strongly with the small domain in human DHODH. Asp242–Thr261 (β5 and loops) and Val287–Glu300 are involved in the dimerization of *Lactococcus* DHODH [15].

The membrane-association motif

An N-terminal extension distinguishes family 1 and family 2 DHODHs. Multiple sequence alignments on the available DHODH sequences show that all known membrane associated DHODH sequences have an N-terminal extension that is missing in all cytosolic ones (Figure 2). In human DHODH, this extension contains the small domain and the loop connecting it to the large domain. In the amphipathic small domain, all of the charged and most of the polar residues orient towards the large domain whereas the hydrophobic sidechains project away from the large domain (Figure 4a). The hydrophobic sidechains of the small domain (Met30, Phe37, Leu49, Leu50, Leu58, Phe62, Leu65 and Leu67) form a large protruding hydrophobic patch (Figure 4a). The positively charged sidechains of residues from the small (Arg36, Arg57, Arg61, His41 and His56) and large (Arg131, Arg372) domains form a positively charged fringe at the base of the hydrophobic protrusion (Figure 4a). There are several salt bridges and hydrogen bonds between the large and small domains, and many of the residues involved (Glu53, His56, Arg133 and Arg136) are completely conserved in family 2 DHODHs (Figure 2).

The small domain's structure suggests its involvement with membrane association. The protruding hydrophobic patch could push into the hydrophobic interior of the membrane while the positively charged periphery would interact with the negatively charged phospholipid head groups. In the crystal structure, a detergent molecule (DDAO) is tightly bound to the center of the hydrophobic patch with its head group oriented towards the edge (Figure 4b). A somewhat similar membrane-binding motif has been observed in the prostaglandin H2 synthase-1 structure, in which three α helices were suggested to interact with the lipid layer [17].

The version of human DHODH used in this work lacks 29 N-terminal amino acids. Knecht *et al.* have suggested that these missing N-terminal residues contain a mitochondrial signal peptide and a possible transmembrane peptide of 18 amino acids [18]. Such a transmembrane peptide could augment the membrane association of human DHODH, and nothing in our analysis excludes such a possibility. However, the transmembrane peptide is not required for membrane association, as shown by Copeland *et al.* [14]. *Escherichia coli* DHODH, which has an N terminus similar to the protein used in our work (Figure 2), is also membrane associated.

The inhibitor-binding region

The space between α1 and α2 forms a 10×20 Å slot in the hydrophobic patch, with the short α1–α2 loop at the narrow end (Figure 4a). This slot forms the entrance to a tunnel that ends at the FMN cavity beneath the α1–α2 loop. This tunnel narrows as it goes into the proximal

Figure 3

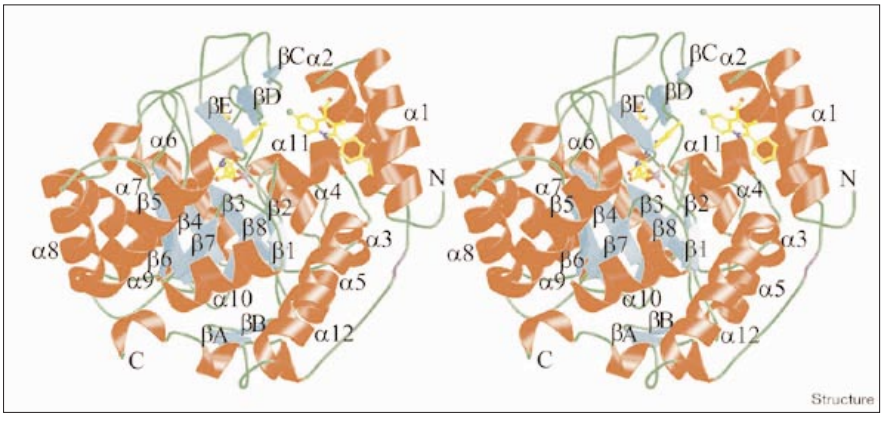

Stereoview ribbon diagram of human DHODH. Helices, strands and coils are colored red, cyan, and green, respectively. Residues with weak electron density are in purple. Ligands (the inhibitor shown here is a brequinar analog) are shown in ball-and-stick representation with yellow carbon, red oxygen, blue nitrogen, pink phosphorus, and green fluorine atoms. Secondary structural elements and the N and C termini are labeled. This figure was prepared using MOLSCRIPT [34].

redox site, and several charged or polar sidechains (Gln47, His56, Tyr356, Thr360 and Arg136) are located at the narrow end of the channel (Figure 4b). Ubiquinone, which can readily diffuse in the mitochondrial inner membrane, undoubtedly uses this tunnel to approach $FMNH_2$ for a redox reaction.

A brequinar analog is located in this channel, with the 6-fluoro-3-methyl-4-quinoline carboxylic acid end of the molecule most deeply buried in the polar environment and the hydrophobic aromatic rings in the hydrophobic part of the channel (Figure 4b). The carboxylate hydrogen bonds to the sidechain of Gln47 and forms a salt bridge with Arg136 (Figure 4b). The only water observed in the channel forms hydrogen bonds with Thr360 Oγ and the carboxylate (Figure 4b). The fluoroquinoline ring stacks with the imidazole ring of His56, and the His56Ala mutant of human DHODH is more than 100-fold less sensitive to brequinar [19]. The 6-fluoro group makes the closest approach to FMN: 3.8 Å to the C7 methyl. The biphenyl group has hydrophobic contacts with the sidechains of Met43, Ala59, Leu68 and Pro364 as well as the detergent molecule in the mouth of the channel (Figure 3c). These extensive interactions might explain brequinar's high affinity for human DHODH [5].

Metabolic studies have indicated that leflunomide is rapidly processed *in vivo* to a primary metabolite A771726, which mediates the immunosuppressive and disease-modifying effects of the parent drug (Figure 1) [20]. A771726 binds to the same site as brequinar (Figure 5a). The carbonyl is hydrogen bonded to a water, which in turn is bound to Arg136, while the enolic OH is hydrogen bonded to Tyr356 (Figure 5a). The trifluoromethyl-containing aromatic ring makes numerous hydrophobic contacts with residues in the tunnel (Figure 5a). There are fewer inhibitor–protein interactions in the A771726 complex than in the brequinar complex because of the smaller size of A771726, and the binding region in the A771726 complex is less ordered than in the brequinar complex.

Both A771726 and brequinar use similar features to bind in the same location, and analysis of these bound inhibitors illustrates how ubiquinone, the natural substrate, would bind in the same channel. The ubiquinone head group overlays well with the brequinar quinoline group and if ubiquinone occupied the same position the two quinone carbonyl oxygens could accept hydrogen bonds from Arg136 and Tyr356. Both Arg136 and Tyr356 are completely conserved in family 2 DHODHs, except for one sequence where the tyrosine residue is one residue further along (Figure 2). Tyr356 and/or the tightly bound water that is observed in the brequinar complex could provide any protons needed to generate a neutral hydroquinone after electron transfer from the FMN.

Figure 4

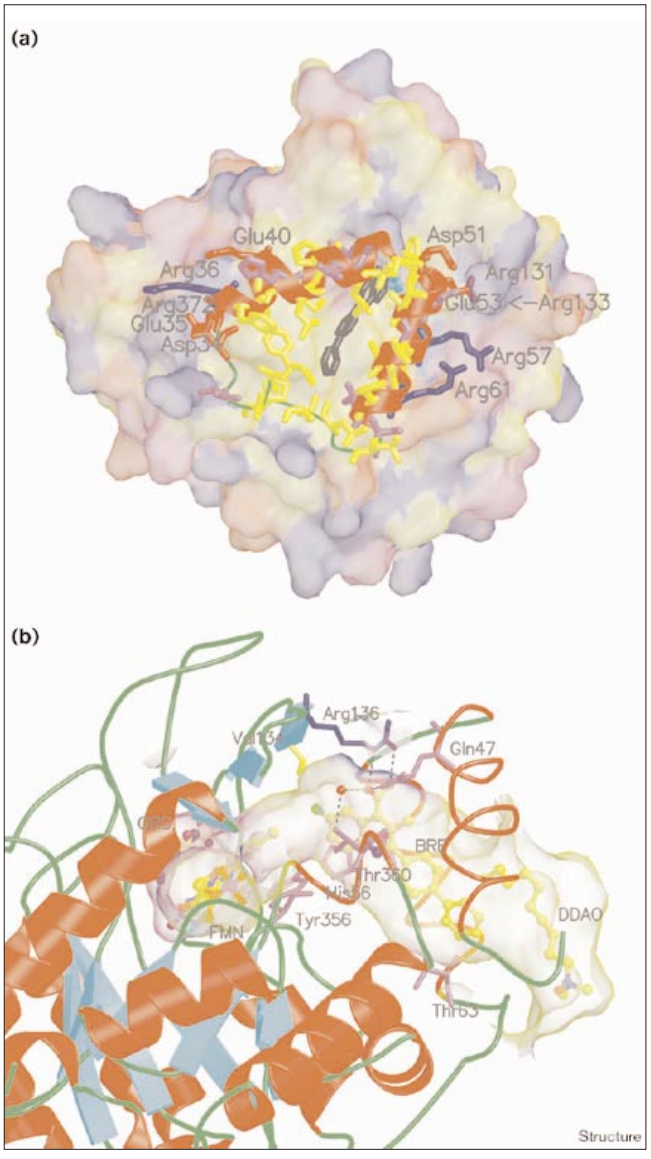

The membrane-binding motif and the inhibitor-binding channel of human DHODH. **(a)** Surface representation of human DHODH. Acidic, basic, polar and hydrophobic residues and surfaces are colored red, blue, magenta and yellow, respectively. Charged residues are labeled. Brequinar and FMN are represented by black and cyan sticks, respectively. This figure was prepared using GRASP [35]. **(b)** The tunnel leading into the proximal redox site of DHODH. The surface of the cavity is colored as in (a). Orotate (ORO) and FMN are bound in the narrow polar region, brequinar is bound in the middle region, and a detergent (DDAO) is bound at the entrance. This figure was prepared using MOLSCRIPT [34].

The structures of the bound inhibitors also highlight key specificity determinants for different members of family 2 DHODHs. For example, mammalian DHODHs are sensitive to brequinar whereas other family 2 DHODHs, most notably the *E. coli* enzyme, are insensitive [5,14].

Val134 in human DHODH is only 3.2 Å from the fluorine of brequinar and 3.9 Å from the methyl of A771726, and the corresponding residue in *E. coli* DHODH is leucine. Model building shows a steric clash with leucine that would prevent ligand binding.

A crucial specificity determinant between family 1 and 2 DHODHs is the hydrophobic channel in which the inhibitors are bound in human DHODH. Family 1 DHODHs simply have no equivalent tunnel, and the edge of FMN is exposed to solvent. But there are other prominent features that discriminate between families 1 and 2, most notably Arg136 and Tyr356 (Figures 2 and 4a). In family 1 DHODHs the Arg136 equivalent is usually aspartate or glutamate (in 9 out of 12 sequences), and the equivalent of Tyr356 is always glycine. The two families could scarcely have more different charge and shape determinants in the critical region near FMN.

The orotate-FMN-binding region

In addition to the tunnel for ubiquinone, the distal electron acceptor, human DHODH has significant changes in the proximal redox site where dihydroorotate and FMN bind (Figure 1). Kinetic studies on the dihydroorotate–orotate exchange reaction using ^{14}C-labeled orotate showed that for *E. coli* DHODH the oxidization of dihydroorotate by FMN is essentially irreversible. On the other hand, the exchange reaction is considerably faster for *Lactococcus* DHODH [21]. Fluorescence studies on bound FMN suggest much tighter binding in *E. coli* DHODH than in *Lactococcus* DHODH [21]. In our structures the aromatic ring of orotate is almost parallel to FMN and is 3.2–3.8 Å from its *si* face (Figure 5b). Orotate's other face is completely covered by the Asn212–Gly226 loop. The location and orientation of orotate in human DHODH is essentially the same as in the *Lactococcus* DHODH–orotate complex structure [16].

Figure 5

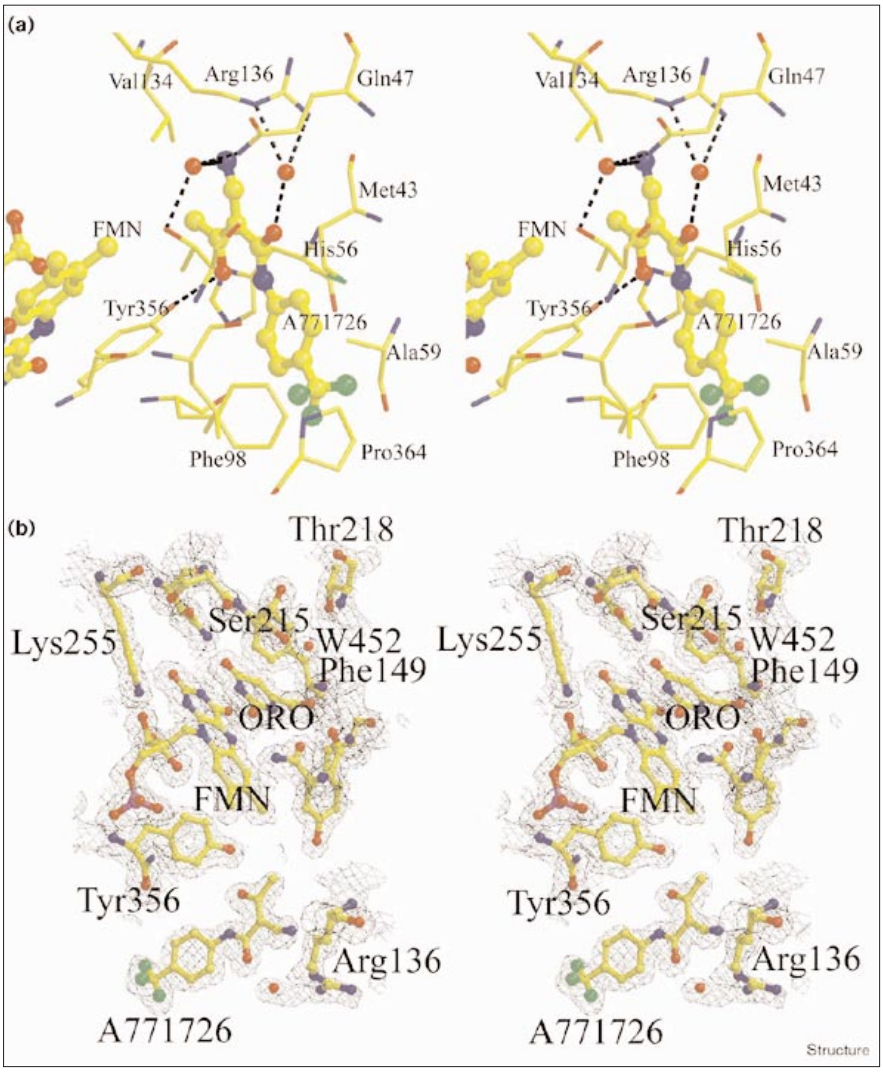

Binding of A771726 in the hydrophobic channel of human DHODH. **(a)** Stereoview of the binding interactions of A771726. Ligands are shown in ball-and-stick representation, and residues interacting with A771726 are represented by thin sticks. Hydrogen bonds are shown as dashed black lines. **(b)** A $2F_o–F_c$ electron-density map of A771726, FMN and orotate contoured at 1.2σ (1.8 Å). Ligands and selected DHODH residues in the vicinity are shown in ball-and-stick representation. This figure was prepared with MOLSCRIPT [34].

The weaker electron density and higher temperature factors of this loop suggest that it opens to admit dihydroorotate and release orotate from a closed active site. There are several highly conserved residues at the ends of this flexible loop. Asn212, Ser214 and Pro216 are conserved in all DHODHs, and in family 2 Leu221, Arg222 and Gln225 are conserved and a leucine/methionine at 224 is conservatively substituted (Figure 2).

Kinetic studies on bovine liver mitochondria DHODH have shown that a general base abstracts a proton from the C5 position of dihydroorotate [22] (Figure 1). The substrate is held in place by two completely conserved asparagine residues (145 and 284), and the closest protein atom to C5 in human DHODH is Ser215 Oγ (3.2 Å) (Figure 5b). Ser215, which is completely conserved in family 2 DHODHs, is essential for catalysis in *E. coli* DHODH, a family 2 member [21]. It's likely that Ser215 plays the role of catalytic base in human DHODH, and such a role would be unusual for a serine. The Oγ of Ser215 hydrogen bonds to a tightly bound water molecule, which in turn hydrogen bonds to Thr218 Oγ1 and the π electron cloud of Phe149 (Figure 5b). Both Thr218 and Phe149 are conserved in family 2 DHODHs, and this series of hydrogen bonds and π interactions could both enhance the basicity of the Ser215 sidechain and stabilize its position during the reaction. In family 1, the catalytic base is cysteine and Thr218 and Phe149 are valine and leucine, respectively [11,16].

In the reduction of FMN to $FMNH_2$, N5 and possibly N1 of the flavin form new N–H bonds (Figure 1). N5 receives the hydride from C6 of dihydroorotate, and the N5–C6 distance of 3.6 Å is compatible with direct hydride transfer (Figures 1 and 5b). N1 could be negatively charged or protonated, and Lys255, which is conserved in all known DHODH sequences but one, could serve either as a proton donor or as a negative charge stabilizer.

FMN and orotate have extensive hydrophobic contacts and form multiple hydrogen bonds with human DHODH. These interactions are generally similar to those observed in the *Lactococcus* DHODH structure [15,16], and several of the interacting residues (Asn145, Gly148, Asn212, Asn284, Gly306 and Gly335) are conserved in all DHODH sequences (Figures 2 and 5b). Others are mostly conserved (Gly97 and Lys225) or conservatively substituted (Thr285Ser and Asn217His). Lys100, which is conserved in family 2 members, forms hydrogen bonds with FMN and the carboxylate of orotate, and Lys43 plays an equivalent role in family 1 DHODHs. Ser120 and Thr357 have a common role in *Lactococcus* and human DHODH.

One major difference between the human and *Lactococcus* DHODH structures is the dimethylbenzene ring of FMN, which is tightly packed against sidechains in the human but not in the bacterial enzyme. In the human enzyme, Asn145, Tyr356 and Tyr147 all cluster about the sides of the dimethylbenzene ring of FMN, and this packing would explain the tighter binding and more negative redox potential of family 2 than family 1 DHODHs [21]. The dimethyl end of the ring is exposed to the hydrophobic channel, and this is presumably the region in which the second redox reaction between $FMNH_2$ and ubiquinone takes place.

In each complex model there is a sulfate ion and an acetate ion. Both ions are located at the protein surface and are far away from either the inhibitor-binding region or the orotate-FMN-binding region.

Biological implications

The structures reported here illuminate two facets of human dihydroorotate dehydrogenase (DHODH): the three-dimensional organization of its catalytic site and the binding motifs of potential therapeutic agents. The first is important for understanding the mechanistic enzymology of pyrimidine biosynthesis; the second will suggest designs for better therapies for diseases characterized by rapidly proliferating cells.

DHODH has two redox sites, one where FMN oxidizes dihydroorotate to orotate and another where ubiquinone oxidizes $FMNH_2$ to FMN. The bound orotate and FMN clearly define one redox site of human DHODH, and it resembles in organization but not in detail the redox site of a bacterial DHODH. The most surprising difference between the human and bacterial enzymes is a serine replacing a cysteine as the catalytic base. This catalytic serine, Ser215, is conserved in family 2 DHODHs. Two other completely conserved residues, Thr218 and Phe149, along with a tightly bound water molecule could function to enhance the basicity of Ser215. A more complete understanding of the catalytic mechanism will require further work.

The structures also reveal that the long N-terminal extension that characterizes family 2 DHODHs forms a helical membrane-associated motif, which forms the mouth of a hydrophobic tunnel leading into the $FMNH_2$–ubiquinone redox site. The inhibitors bind to a narrow region in this tunnel, and this location has interesting implications for structure-based drug design. Leo Tolstoy's well-known description of families — "All happy families resemble one another, each unhappy family is unhappy in its own way" — finds an analogy in enzymes. All DHODH active sites resemble one another. They must because they all carry out the same reaction. Regions near active sites can differ. In human DHODH the residues that interact with the inhibitors differ markedly from one organism to another, and a single residue change can confer resistance. Future ther-

apeutic agents, both those targeted to rapidly proliferating human cells and those targeted to human pathogens, could be designed to explicitly exploit these differences.

Materials and methods

Protein expression and purification

The cDNA encoding an N-terminally truncated human DHODH (Met30–Arg396) was amplified by the polymerase chain reaction (PCR) and cloned into pET-19b plasmid (Novagen, Madison, WI). The vector produces human DHODH as an N-terminal ten-histidine fusion protein. The plasmid pET-19b–human DHODH was transformed into BL21 (DE3) pyrD *E. coli* cells for protein production. Cells were grown at 25°C in a rich medium [23], and were induced with 1 μM isopropyl-β-D-thiogalactoside at an OD_{600} of 0.6–0.8. Cells were harvested after an additional 20 h of growth. A cell pellet from 1 l of culture was lysed in 100 ml of buffer A (50 mM HEPES pH 7.7, 300 mM NaCl, 10% glycerol). Triton X-100 was added to a final concentration of 1% into the lysate before centrifugation at 48,000 × g for 30 min. The supernatant was incubated with 3 ml TALON beads (Clontech) for an hour. Triton X-100 was exchanged by washing with 10 mM *N*,*N*-dimethylundecylamine-*N*-oxide (C11DAO) in buffer A. Step gradients of imidazole (0, 16, 30 and 160 mM in buffer A) were used to elute DHODH. DHODH began to elute with 30 mM imidazole, as indicated by the appearance of a yellow color in the eluate. At this point, pure DHODH was rapidly eluted with 160 mM imidazole. The yield of pure DHODH was typically 40 mg/l of culture. Selenomethionine incorporation into human DHODH was expressed as described in [24] and purified as above. The His_{10} tag was not removed for further studies.

Crystallization and data collection

Human DHODH was co-crystallized with a brequinar analog or A771726 at 20°C using the hanging-drop diffusion method. Drops were formed by mixing equal amounts of 20 mg/ml protein in 10 mM C_{11}DAO, 400 mM NaCl, 30% glycerol, 1 mM EDTA, 50 mM HEPES pH 7.7, with a precipitant solution of 0.1 M acetate pH 4.8, 40 mM C_{11}DAO, 20.8 mM *N*,*N*-dimethyldecylamine-*N*-oxide (DDAO), 2 mM DHO 2.4–2.6 M ammonium sulfate, 1 mM brequinar analog or A771726, against 1 ml reservoir of 0.1 M acetate pH 4.8, 2.4–2.6 M ammonium sulfate, 30% glycerol. Crystals usually appeared in three days and reached the full size of 0.15 × 0.15 × 0.15 mm in two weeks. It was observed that detergent DDAO, substrate dihydroorotate (or product orotate) and inhibitor were all necessary for crystallization. The crystals belonged to space group $P3_221$, with $a = b = 90.61$ and $c = 122.41$ Å. Crystals were flash frozen in liquid nitrogen. During data collection crystals were kept at 100K in a cool nitrogen stream. Single wavelength crystal data were collected at CHESS A1. MAD data were collected at CHESS F2 on a SeMet crystal complexed with brequinar. The reflection intensities were integrated and processed using the CCP4 program suite [25] (Table 1). The 2′-desfluoro brequinar analog used in this study has essentially the same potency against human DHODH and the human mixed lymphocyte reaction as brequinar (data not shown).

Structure determination and refinement

A phasing model of the brequinar complex was found using the MAD phasing method. Direct methods (SHELXL-97) [26] found four of the five selenium positions from the MAD |λ1–λ3| dispersive signal. All selenium atoms were confirmed by self- and cross-vector peaks on the anomalous and dispersive Patterson maps, which were virtually noise free. Selenium position refinement and phase calculations were carried out with MLPHARE [27]. The electron-density map was improved by a solvent-flattening and histogram-matching method using the DM program [28]. The experimental map was so excellent that brequinar, FMN and ORO are clearly interpretable and the mainchain and sidechain atoms of all protein residues except two flexible loops, Arg70–Arg72 and Arg222–Gln225, can be identified. The initial brequinar complex model was built into the electron-density map using the program O [29] and refined against all available reflection data using the programs CNS [30] and REFMAC [31]. In the final brequinar complex model there are 2760 protein atoms, one molecule of brequinar analog, FMN, detergent DDAO and ORO, a sulfate and an acetate ion, and 288 water molecules. The model is well refined and has good geometry (Table 1). The A771726 complex structure was solved using the difference Fourier method. A771726 was located in the electron-density map phased with the brequinar complex model,

Table 1

Data collection and refinement statistics.

Crystal	SeMet	Brequinar	A771726
X-ray source	CHESS F2	CHESS A1	CHESS A1
Wavelength (Å)	0.9792/0.9790/0.9633	0.936	0.9134
Resolution (Å)	2.0	1.6	1.8
Observations	305,531/305,836/305,526	444,987	264,642
Unique reflections	39,802/39,841/39,806	75,457	54,515
Completeness	99.4 (100)/99.4 (100.0)/99.3 (100)	97.1 (84.8)	99.0 (99.8)
Redundancy	7.7/7.7/7.7	5.9	4.9
R_{sym}	8.5 (28.9)/8.9 (32.0)/8.3 (28.2)	4.0 (21.0)	7.9 (20.4)
Phasing (SeMet MAD)			
$R_{dispersive}$ (%)	λ1–λ3: 5.1/λ2–λ3: 4.5		
R_{anom} (%)	4.2/4.2/3.5		
FOM* (before DM)	0.489 (0.174)		
FOM* (after DM)	0.736 (0.544)		
Refinement			
R factor (%)		16.9 (16.6)	16.2 (17.6)
R_{free} (%)		18.8 (19.4)	18.5 (20.7)
Bond length (Å)		0.009	0.01
Bond angle (°)		2.0	2.2

Values in parentheses are for the highest resolution data: 2.0–2.1 Å for SeMet, 1.8–1.9 Å for A771726, and 2.0–2.1 Å for brequinar. *FOM, figure of merit.

with brequinar and water molecules removed. The final model was well refined against all available data with good geometry (Table 1). There are 2778 protein atoms, one molecule of A771726, FMN and ORO, a sulfate and acetate ion, and 297 water molecules in the final A771726 complex model. In both the brequinar and A771726 complex structures, loop Arg70–Arg72 is disordered. Loop Asn212–Gly226 has higher temperature factors and has different conformations in different crystals. Within this loop, Arg222–Gln225 is missing in the brequinar complex but is visible in the A771726 complex structures. The His_{10} tag and the linker peptide are not visible in all models.

Accession numbers

The coordinates of both complexes have been deposited in the Protein Data Bank with accession codes 1D3G and 1D3H.

Acknowledgements

This work was partially supported by a USPHS grant to JC (CA590221). We thank J Widom for help with protein expression and purification, T Begley for helpful discussions, and the MacCHESS staff for help in data collection.

References

1. Jones, M.E. (1980). Pyrimidine nucleotide biosynthesis in animals: genes, enzymes, and regulation of UMP biosynthesis. *Annu. Rev. Biochem.* **49**, 253-279.
2. Fairbanks, L.D., Bofill, M., Ruckemann, K. & Simmonds, H.A. (1995). Importance of ribonucleotide availability to proliferating T-lymphocytes from healthy humans. *J. Biol. Chem.* **270**, 29682-29689.
3. Ruckemann, K., *et al.,* & Simmonds, H.A. (1998). Leflunomide inhibits pyrimidine *de novo* synthesis in mitogen-stimulated T-lymphocytes from healthy humans. *J. Biol. Chem.* **273**, 21682-23691.
4. Williamson, R.A., *et al.,* & Ruth, E. (1995). Dihydroorotate dehydrogenase is a high affinity binding protein for A771726 and mediator of a range of biological effects of the immunomodulatory compound. *J. Biol. Chem.* **270**, 22467-22472.
5. Chen, S.F., Perrella F.W., Behrens, D.L. & Papp, L.M. (1992). Inhibition of dihydroorotate dehydrogenase activity by brequinar sodium. *Cancer Res.* **52**, 3521-3527.
6. Peters, G.J., Nadal, J.C., Laurensse, E.J., de Kant, E. & Pinedo, H.M. (1990). Retention of in vivo antipyrimidine effects of Brequinar sodium (DUP-785; NSC 368390) in murine liver, bone marrow and colon cancer. *Cancer Res.* **50**, 4644-4649.
7. Joshi, A.S., *et al.,* & Kornhauser, D.M. (1997). Phase I safety and pharmacokinetic studies of brequinar sodium after single ascending oral doses in stable renal, hepatic, and cardiac allograft recipients. *J. Clin. Pharmacol.* **37**, 1121-1128.
8. Dimitrijevic M. & Bartlett R.R. (1996). Leflunomide, a novel immunomodulating drug, inhibits homotypic adhesion of peripheral blood and synovial fluid mononuclear cells in rheumatoid arthritis. *Inflamm. Res.* **45**, 550-556.
9. Silva, H.T., Jr & Morris, R.E. (1997). Leflunomide and malononitrilamides. *Am. J. Med. Sci.* **313**, 289-301.
10. Smolen, J.S., *et al.*, & Rosenburg, R. (1999). Efficacy and safety of leflunomide compared with placebo and sulphasalazine in active rheumatoid arthritis: a double-blind, randomised, multicentre trial. European Leflunomide Study Group. *Lancet* **353**, 259-266.
11. Bjornberg, O., Rowland, P., Larsen, S. & Jensen, K.F. (1997). Active site of dihydroorotate dehydrogenase A from *Lactococcus lactis* investigated by chemical modification and mutagenesis. *Biochemistry* **36**, 16197-16205.
12. Nagy, M., Lacroute, F. & Thomas, D. (1992). Divergent evolution of pyrimidine biosynthesis between anaerobic and aerobic yeasts. *Proc. Natl Acad. Sci. USA* **89**, 8966-8970.
13. Minet, M., Dufour, M & Lacroute, F. (1992). Cloning and sequencing of a human cDNA coding for dihydroorotate dehydrogenase by complementation of the corresponding yeast mutant. *Gene* **121**, 393-396.
14. Copeland, R.A., *et al.,* & Patterson, T.A. (1995). Recombinant human dihydroorotate dehydrogenase: expression, purification, and characterization of a catalytically functional truncated enzyme. *Arch. Biochem. Biophys.* **323**, 79-86.
15. Rowland, P., Nielsen, F.S., Jensen, K.F. & Larsen, S. (1997). The crystal structure of the flavin containing enzyme dihydroorotate dehydrogenase A from *Lactococcus lactis*. *Structure* **5**, 239-252.
16. Rowland, P., Bjornberg, O., Nielsen, F.S., Jensen, K.F. & Larsen, S. (1998). The crystal structure of *Lactococcus lactis* dihydroorotate dehydrogenase A complexed with the enzyme reaction product throws light on its enzymatic function. *Protein Sci.* **7**, 1269-1279.
17. Picot, D., Loll, P.J. & Garavito, R.M. (1994). The X-ray crystal structure of the membrane protein prostaglandin H2 synthase-1. *Nature* **367**, 243-249.
18. Knecht, W., Bergjohann, U., Gonski, S., Kirschbaum, B. & Loffler, M. (1996). Functional expression of a fragment of human dihydroorotate dehydrogenase by means of the baculovirus expression vector system, and kinetic investigation of the purified recombinant enzyme. *Eur. J. Biochem.* **240**, 292-301.
19. Davis, J. & Copeland, R.A. (1997). Histidine to alanine mutants of human dihydroorotate dehydrogenase. Identification of a brequinar-resistant mutant enzyme. *Biochem. Pharmacol.* **54**, 459-465.
20. Bartlett, R.R., *et al.*, & Bremer, E. (1991). Leflunomide (HWA 486), a novel immunomodulating compound for the treatment of autoimmune disorders and reactions leading to transplantation rejection. *Agents Actions* **32**, 10-21.
21. Bjornberg, O., Gruner, A.C., Roepstorff, P. & Jensen, K.F. (1999). The activity of *Escherichia coli* dihydroorotate dehydrogenase is dependent on a conserved loop identified by sequence homology, mutagenesis, and limited proteolysis. *Biochemistry* **38**, 2899-2908.
22. Hines, V. & Johnston, M. (1989). Mechanistic studies on the bovine liver mitochondrial dihydroorotate dehydrogenase using kinetic deuterium isotope effects. *Biochemistry* **28**, 1227-1234.
23. Yang, Q.H., Wu, C.L., Lin, K. & Li, L. (1997). Low concentration of inducer favors production of active form of 6-phosphofructo-2-kinase/fructose-2,6-bisphosphatase in *Escherichia coli*. *Protein Exp. Purif.* **10**, 320-324.
24. Doublie, S. (1997). Preparation of selenomethionyl proteins for phase determination. *Methods Enzymol.* **276**, 523-530.
25. Collaborative Computational Project, Number 4. (1994). The CCP4 Suite: programs for Protein Crystallography. *Acta Crystallogr. D* **50**, 760-763.
26. Sheldrick, G.M. (1997). Patterson superposition and *ab initio* phasing. *Methods Enzymol.* **276**, 628-641.
27. Otwinowski, Z. (1991). Maximum likelihood refinement of heavy atom parameters. In *Isomorphous Replacement and Anomalous scattering,* (Wolf, W., Evans, P.R. & Leslie, A.G.W., eds) *Daresbury Laboratory, Daresbury, UK.*
28. Cowtan, K.D. & Main, P. (1998). Miscellaneous algorithms for density modification. *Acta Crystallogr. D* **54**, 487-493.
29. Jones, T.A., Zou, J.Y., Cowan, S.W. & Kjeldgaard, M. (1991). Improved methods for binding protein models in electron density maps and the location of errors in these models. *Acta Crystallogr. A* **47**, 110-119.
30. Brünger, A.T., *et al.,* & Warren, G.L. (1998). Crystallography & NMR system: A new software suite for macromolecular structure determination. *Acta Crystallogr. D* **54**, 905-921.
31. Murshudov, G.N., Vagin, A.A., Lebedev, A., Wilson, K.S. & Dodson, E.J. (1999). Efficient anisotropic refinement of macromolecular structures using FFT. *Acta Crystallogr. D* **55**, 247-255.
32. Thompson, J.D., Higgins, D.G. & Gibson, T.J. (1994). CLUSTALW: improving the sensitivity of the progressive multiple sequence alignment through sequence weighting, position specific gap penalties and weight matrix choice. *Nucleic Acids Res.* **22**, 4673-4680.
33. Baton, G.J. (1993). ALSCRIPT: a tool to format multiple sequence alignment. *Protein Eng.* **6**, 37-40.
34. Kraulis, P.K. (1991). MOLSCRIPT: a program to produce both detailed and schematic plots of protein structures. *J. Appl. Crystallogr.* **24**, 946-950.
35. Nicholls, A., Sharp, K.A. & Honig, B. (1991). Protein folding and association: insights from the interfacial and thermodynamic properties of hydrocarbons. *Proteins* **11**, 282.